FARADAY

Voids in network-forming liquids and their influence on the structure and dynamics

Mark Wilson,[a] Paul A. Madden,[a] Nikolai N. Medvedev,[b] Alfons Geiger[c] and Andreas Appelhagen[c]

[a] *Physical and Theoretical Chemistry Laboratory, Oxford University, South Parks Road, Oxford, UK OX1 3QZ*

[b] *Russian Academy of Science, Institute of Chemical Kinetics and Combustion, Novosibirsk 630090, Russia*

[c] *Physical Chemistry, University of Dortmund, D-44221 Dortmund, Germany*

A Voronoi analysis is applied to clarify the origin of certain unusual physical properties of three representative network-forming ionic liquids: SiO_2, $ZnCl_2$, and $BeCl_2$. In each of these fluids, the local structure under ambient pressure comprises a tetrahedral unit of anions around cations which link together to form a network. The Voronoi analysis is used to characterize the empty space (voids) within the network. Despite sharing the same local tetrahedral arrangement, the network properties of the three liquids differ markedly on an intermediate length scale and this leads to significant differences in the properties of the voids. It is shown how the void analysis helps to interpret the anomalous behaviour of the diffusivity in SiO_2, which over a certain range of density increases with increasing density, and to clarify the origin of the intermediate range order in the atomic positions, as seen in the much discussed first sharp diffraction peak (or prepeak) in diffraction data.

1 Introduction

Computer simulation 'experiments' offer a unique insight into the nature of a variety of chemically distinct systems. Atom positions and velocities are known unequivocally for a given model and so offer unlimited scope for probing the microscopic detail which underlies observable phenomena. However, as the quantity of information available from such simulations itself leads to analytical problems, it may require a major effort to extract the desired insight. Clearly such problems increase as system sizes increase with computer power. New measures must be introduced to condense the information to a manageable level. These measures are often unfamiliar and introduced for subjective reasons (unlike directly observable quantities like correlation functions or structure factors) and their relationships to observables must be established.

These problems may be compounded in systems in which multiple length scales are significant. Many systems of stoichiometry MX_2 can be understood, at a static structural level, in terms of the linking of MX_4 tetrahedra. Such tetrahedra may link together in three ways (or a mixture thereof) through a single anion bridge (corner-sharing), a double anion bridge (edge-sharing), or a triple bridge (face sharing), the latter being relatively rare in nature. For example, the structure of SiO_2 is dominated by corner-sharing SiO_4 tetrahedra which link together to form a three-dimensional network. Subtle features of these polyhedral linkages (in particular the Si—O—Si bond angle) lead to a second (longer) length scale than that of the anion–cation ordering imposed by the system ionicity. Such intermediate-ranged order (IRO) requires different structural probes for full characterization compared to the close-packed or coulomb-ordered structures typical of Lennard-Jones or simple ionic systems. For example, the network nature of these systems leads to an inherent ring structure. Also, unlike close-packed systems, they show a propensity for supporting regions of empty space (voids). The manner in which this empty space is organised by elementary interactions and is responsible for some observable characteristics of the liquids is the subject of this paper.

Recent work, using a polarizable-ion model (PIM) which incorporates anion dipole polarization effects, has shown how the spatial relationship between the MX_4 tetrahedra is largely controlled by the anion dipole polarization.[1] Dipoles induced on the bridging anions introduce electron density in between pairs of cations centred in neighbouring polyhedra, which act to screen the repulsive coulombic cation–cation interaction and so control the M—X—M triplet bond angle. The magnitude of this effect (and hence the bond angle itself) is controlled not only by the anion polarizability but also by the cation charge and the anion–cation separation, the latter two controlling the size of the polarizing electric field at the anion site. For relatively unpolarizable anions such as O^{2-} the effect is subtle with many static structural properties (within a single phase) reproducible using a simple rigid-ion model (RIM), i.e. a classical pair potential.[2] At the other extreme $BeCl_2$ is an example in which the combination of a polarizable anion with a small (highly polarizing) cation leads to massive polarization effects which bend the M—X—M triplet to such an extent as to stabilize edge over corner-sharing.[1,3] For Cl^- with a somewhat larger cation (such as Zn^{2+}) an SiO_2-like corner-sharing network (with limited edge-sharing) is generated, but the M—X—M bond angle is considerably more acute than in SiO_2 which has important consequences in the IRO.

In the present work only voids within the cation subdensity distribution are considered as the cations are the centres of the interconnected tetrahedra and, as a result, define their spatial arrangement. It is now well understood that fluctuations in the cation density are significant in defining an intermediate-ranged length scale in a wide variety of systems. Coupled to the emergence of this second length scale is the first sharp diffraction peak (FSDP), a peak in the static structure factor which appears at a scattering angle significantly smaller than that of the principal peak. Such a peak arises in both the cation–cation and void–void structure factors for $ZnCl_2$.[4] However, it is not clear that such an association of cation density fluctuations and void fluctuations should appear in all tetrahedron-based systems from $BeCl_2$-like to SiO_2-like.

A remarkable feature of tetrahedral network liquids is the

fact that over certain regions of density, the diffusivity of the ions increases with increasing density. Work with a RIM has shown how the five-coordinate Si^{4+} sites appear as important 'intermediates' in the diffusion process (see, for example, ref. 2 and references therein). Under pressure or tension a liquid could choose to change the volume of the empty space whilst preserving its network connectivity, or to alter the coordination number of the ions. It is therefore of interest to examine the relationship between changes in void size and spatial distribution induced by changes in the applied pressure and the corresponding changes in the observable diffusivity. This type of structural analysis has been applied extensively to the study of water (see, for example, ref. 5 and references therein) with the similarity of 'network' systems such as water and silica being the subject of ongoing debate.[6]

2 Methods

2.1 Potential models

Here we consider molecular dynamics simulations of models of $ZnCl_2$, $BeCl_2$ and SiO_2. In all cases the interactions are described as the sum of (Born–Mayer) pair potentials plus an account of anion polarization *via* the polarizable-ion model (or PIM).[1] Omitting the polarization terms, leaving only the pair potentials, gives the rigid-ion model (RIM) for that substance, whose predicted properties may usefully be compared and contrasted with those of the PIM. Omitting the polarization effects simplifies the connectivity of the polyhedral network, as the intermediate range structure becomes dominated by the effects of the coulombic repulsion between the more highly charged cations. The $ZnCl_2$ and $BeCl_2$ models have been described previously[3,7] whilst a modified SiO_2 potential from ref. 8 is used.[9] Cation polarization effects are assumed to be insignificant as the bare cation polarizabilities are much smaller than those of the anions and, furthermore, the cations tend to be at the centre of high symmetry polyhedra which preclude low order polarization effects. It should be stressed that these interaction potentials are not presented as quantitatively accurate models for these systems, but rather as models which recapture the distinctive aspects of the interionic correlations. This is particularly the case for SiO_2 in which the nature of the oxide ion requires a more complex model, incorporating coordination environment induced changes in the ion shape.[10–14] For example, a deficiency of the present SiO_2 model is that the ion motion appears to be too rapid when compared to experimental viscosity data.

The basic Born–Mayer parameters for the three models are listed in Table 1 with the polarization parameters listed in Table 2. The latter consist of a dipole anion polarizability and a short-range damping parameter, which reflects the effect of cation–anion overlap on the induced dipoles.[1]

2.2 Voronoi analysis

Our assignment of voids in the spatial arrangement of the ions is based upon a Voronoi analysis, a description of which appeared in ref. 15, for example. In a topologically disordered structure the vertices of the Voronoi polyhedra (VP) define a group of four atoms and are known as the Delauney simplices (DS). About each DS a circumsphere can be constructed which passes through these four atoms such that no other atom centre lies within that circumsphere. As a result the distribution of circumsphere radii is a measure of the empty (void) space in the system and yields information not readily accessible from a consideration of the ion positions alone. Further information is available from the relative positions of the voids in real and reciprocal space. Such a method has recently been applied to characterize the empty space in Lennard-Jones systems,[16] to try to understand if a superheated liquid has intrinsic weak points which might serve as bubble nucleation sites. Both voids and ions may be separated into different classes (or 'coloured') on the basis of the values of particular properties, such as the circumsphere radius or the coordination number of an ion.[15,17] Knowledge of the relative positions of suitably coloured voids and ions allows one to address particular questions which arise in identifying the mechanism responsible for some physical observation.

Table 1 Born–Mayer short-range pair potential parameters for the three systems studied

ion pair	a/a_0	B/E_h
Cl—Cl	1.00	8.02
Zn—Cl	1.60	48.05
Cl—Cl	1.66	120.0
Be—Cl	1.90	55.35
O—O	1.30	5.40
Si—O	1.82	66.72

Table 2 Dipole polarizabilities and short-range damping parameters for the three systems studied

ion pair	b/a_0^{-1}	α/a_0^3
$BeCl_2$	1.86	20.0
$ZnCl_2$	1.55	20.0
SiO_2	1.55	10.396

3 A corner-sharing network—SiO_2

At ambient pressures amorphous silica consists of corner-linked SiO_4 tetrahedra, this local structure is a property of the radius ratio of the ions and coulomb charge-ordering. It is reproduced by a simple RIM[8] in the density range of interest (2.0–2.5 g cm^{-3}). The introduction of anion polarization effects in this density range reduces the Si—O—Si bond angle (which tends towards linear in the RIM because of the strong coulomb repulsion between the highly charged cations) and also softens the Si—O—Si triplet bending motion.[1,9] Generally speaking, polarization effects tend to screen the coulombic interactions, and alter the network connectivity. In the crystalline phase, SiO_4 tetrahedra may link together in a variety of ways leading to the relatively large number of SiO_2 polymorphs, such as quartz and cristobalite. Polarization effects play a very important role in determining the relative stability of these different phases.[1,11] At high pressures (density *ca.* 4.2 g cm^{-3}) SiO_2 forms the six-coordinate stishovite phase. A consideration of the crystalline polymorphs of SiO_2 indicates the significance of the empty space in such materials. Quartz, the energetically favoured four-coordinate structure, is already *ca.* 50% less dense than the almost close-packed stishovite structure. Other four-coordinate structures include the zeolites where the molar volumes may be as much as 100% greater than in quartz. Remarkably, given the great difference in molar volumes, the lattice energies of these structures differ by, at most, tens of kJ mol^{-1} in a total lattice energy of over 10 000 kJ mol^{-1}.[18] From the viewpoint of our void analysis then, we expect SiO_2 to support stable voids of a range of sizes and spatial arrangements. This is unlike a Lennard-Jones system, which is always likely to force larger voids to aggregate, in order to reduce the total surface energy.[16]

In the amorphous phase, the dependence of the coordination number on density is believed to parallel that of the underlying crystalline phases: this is experimentally observable in GeO_2, a structural analogue of SiO_2, in which the transition in coordination number takes place over a wide

pressure range with large hysteresis.[19] The linked tetrahedral network nature of the liquid and the glass at ambient pressures leads to the 'strong' glass behaviour of the system.[20] It is now well understood that the high pressure (six coordinate Si) systems are much more 'fragile',[21] that is, they behave much more like typical ionic systems. Under tension amorphous silica readily cavitates to form fractal networks of reduced dimensionality (aerogels).[22]

3.1 Void and coordination number analysis

A series of simulations were performed with the PIM at different temperatures and densities from *ca.* 1.1 g cm^{-3} (around half the ambient pressure experimental density) to *ca.* 5.2 g cm^{-3} (above the density of the high pressure stishovite phase of *ca.* 4.2 g cm^{-3}) and from 2500 to 12 000 K. At each density 25 ps runs were used to collect the statistics; this has previously been shown to be sufficient at these elevated temperatures.[2]

Fig. 1 shows the probability distribution for obtaining a circumsphere of radius σ, $n(\sigma)$ in a series of simulations at different densities. Fig. 2 shows the distribution of cation coordination numbers calculated in the same series of runs using the position of the first minimum in the anion–cation pair distribution function as the cutoff. As indicated in the Introduction, it is of interest to see whether the structure adapts to the change in the density by variation of the nature of the local coordination polyhedra (from the preferred tetrahedral to some other) or by changing the connectivity of the polyhedral network, with the latter best indicated by the change in the voids in the cation distribution.

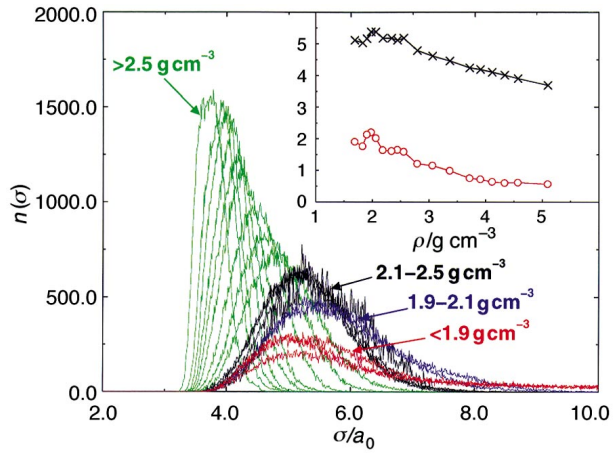

Fig. 1 Circumsphere radii distribution for the SiO_2 model over a range of densities. The distributions are divided into four regions as described in the text. The inset shows the FWHM (red circles) and peak positions (black crosses) at each density.

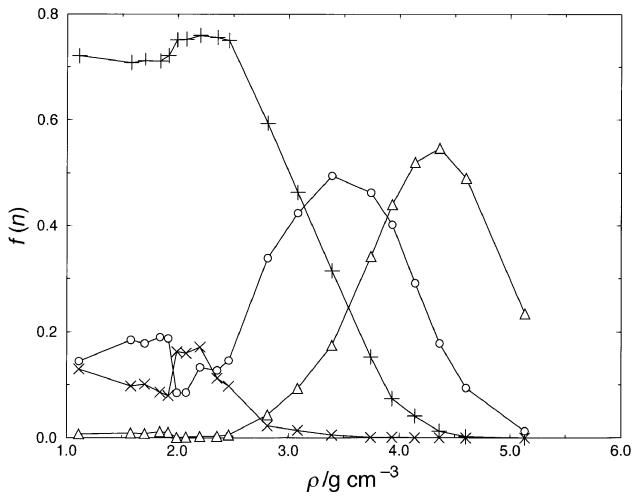

Fig. 2 Fraction of cations with a given coordination number in SiO_2 taken over 25 ps of molecular dynamics as a function of densities. Key: (×) three-coordinate, (+) four-coordinate, (○) five-coordinate, (△) six-coordinate.

Fig. 1 and 2 are immediately suggestive of two distinctive responses to a change of density above and below a critical density of *ca.* 2.5 g cm^{-3}.

Above 2.5 g cm^{-3}, in what we will call region 1, the number of four-coordinate Si centres falls steadily with increasing density and is accompanied by a progressive increase in the number of five- and six-coordinate centres, so that at about 4.0 g cm^{-3} six-coordination predominates. The circumsphere radius distribution is a sharp near-Gaussian with small mean radius and narrow width compared with the lower densities, and both mean radius and width become progressively smaller as the density increases (as shown in the insert to Fig. 1). In this régime, the structure responds to the applied pressure by both increasing the mean coordination number and by making the voids smaller and more uniform in shape and size. This might be thought of as normal 'ionic' behaviour, with the fluid not exhibiting a strong preference for a particular local structure. Rather it accommodates the change in density by a combination of increasing coordination number and decreasing void size.

Below 2.5 g cm^{-3}, the strong preference for tetrahedral coordination is prevalent. The Si centres are predominantly four-coordinate and the number of four-coordinate centres exhibits only a small change with density; from the lowest density up to 2.5 g cm^{-3} the increase in density seems to be accommodated by a change in the shape of the circumsphere radius distribution, with a smaller effect on the most probable radius. Closer inspection of Fig. 1 suggests a further subdivision of the <2.5 g cm^{-3} régime into three regions of different behaviour.

Region 2 ($2.5 > \rho > 2.1$ g cm^{-3}, black lines in Fig. 1) is the region about the ambient pressure density. Across this region the proportion of four-coordinated sites remains constant and the number of three-coordinate sites increases at the expense of five-coordinate ones as the density is lowered. The circumsphere radius distribution is significantly broader, and the mean void size larger than above 2.5 g cm^{-3}. As we shall see, these properties are determined by the intermediate range order in the tetrahedral network.

Moving to slightly lower densities, into region 3 ($2.1 > \rho > 1.9$ g cm^{-3}, blue lines in Fig. 1), the liquid comes under tension. Through this region the ratio of five- to three-coordinate sites decreases with decreasing density. The reduction in density seems to be taken up by an increase in the mean void size, as the most probable radius shifts upwards, and there is also some skewing of the distribution towards larger radii. This therefore corresponds to a region in which the network is stretched without yielding.

Region 4 ($2.1 > \rho > 1.9$ g cm^{-3}, red lines in Fig. 1) corresponds to the region below the mechanical stability limit of the fluid, where it has cavitated under extreme tension. Here the most probable void radius shifts back to its position in the ambient pressure fluid, whilst the distribution develops a long high radius tail associated with the formation of the cavities. The number of each coordination site remains roughly constant and similar in value to the ambient pressure fluid.

3.2 Relationship to the observed diffusivity

Fig. 3 shows the cation diffusion constants (expected to be the observable consequences of this microstructural behaviour) over a limited density and temperature range, corresponding to regions 2 to 4. The diffusion constants were calculated from

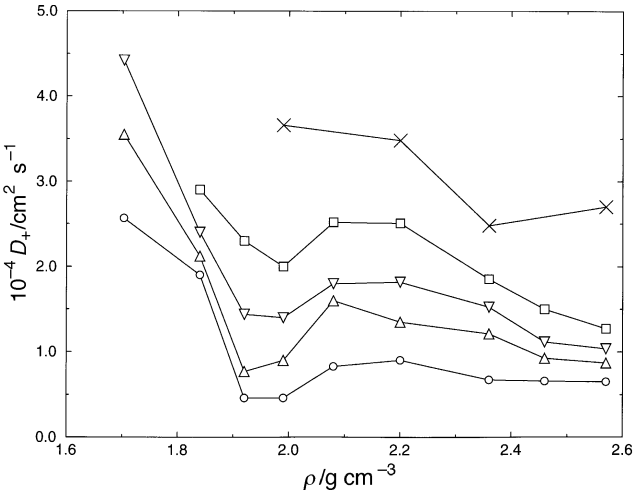

Fig. 3 Si^{4+} cation diffusivity in SiO_2 as a function of density over a range of temperatures. Key: (×) 12 000 K, (□) 9000 K, (▽) 8000 K, (△) 7000 K, (○) 6000 K.

the slopes of the long-time linear regions of the mean squared displacement plotted *vs.* time. Fig. 3 shows the anomalous behaviour of the diffusivity, increasing with increasing density, in what corresponds to region 3 of the earlier discussion. In the high density region 1 and the very low density region 4 the normal decrease of the diffusion coefficient with increasing density is observed, albeit with very different rates and apparent activation energies.

The analysis of the voids and local structures and their spatial distributions *via* the DS construction allows us to understand these observations (Fig. 3) more insightfully. Under ambient conditions (region 2) the four-coordinate Si^{4+} sites are dominant with a significant number of three- and five-coordinate sites. The latter have been proposed as 'intermediates' in the ion diffusion process.[2] As the system density is increased (moving from region 2 to 1) the characteristic narrowing of the circumsphere radii distribution is directly correlated with the collapse of the four-coordinate Si^{4+} tetrahedron-based network to form a more close-packed ionic liquid and is associated with the strong to fragile transition that occurs in SiO_2 as the pressure is increased.[21] Passing from region two to three the number of four-coordinate sites remains approximately constant. There is, however, a significant drop in the number of five-coordinate sites (from *ca.* 14% at 2.2 g cm^{-3} to *ca.* 8% at 2.0 g cm^{-3}) and this is correlated with the dip in diffusivity in Fig. 3. In terms of Fig. 1 this behaviour can now be understood in terms of the initial stretching of the tetrahedral network as the system is placed under tension. For a limited applied negative pressure the network can respond by stretching the Si—O bonds and, to a much greater extent, increasing the Si—O—Si bridging bond angles, thus changing the spatial relationship between neighbouring tetrahedra and altering the IRO. Both of these responses lead to a general increase in void size although the structure retains the essential features of the ambient pressure topology and dimensionality. As a result the circumsphere distribution appears as that at ambient pressure but slightly shifted to larger void sizes.

As the density is reduced below the point of mechanical instability (region 4) the coordination number and circumsphere radius distributions are indicative of the decomposition of the fluid into cavities and regions of bulk-like network whose structure is largely like that at the ambient density. At this point the material has formed a fractal like structure with reduced dimensionality.[22] The expanded network in region 3 is of higher energy than the normal network but is held by the uniform applied pressure. Once the system has cavitated, however, the system is under no such three-dimensional constraint and so regions can 'snap back' to form bulk-like structure. Such behaviour is typical of the stretching of polymers which exhibit a finite amount of resistance to stretching but then catastrophically fails to form macroscopic holes. Fig. 2 shows that the number of five-coordinate sites returns to the ambient pressure values as the three-dimensional network collapses which again appears to be correlated with a rise in the ion diffusivity in Fig. 3.

It is of interest to understand the relationship of the five-coordinate sites to the voids in the cavitated systems. We can ask whether the enhanced diffusion, relative to the perfect four-coordinate structure, is occurring on the surfaces of the cavities or in the bulk-like regions in between them. To this end we define a pair distribution function in terms of the spatial distribution between voids and specific coordination number cations.

$$4\pi r^2 g_{\mathrm{cV}}(r,\sigma_{\mathrm{cut}}) = \frac{V}{(N_{\mathrm{voids}}^{\sigma_{\mathrm{cut}}} N_{\mathrm{sites}}^{\mathrm{CN}})^{1/2}} \sum_{i=1}^{N_{\mathrm{voids}}^{\sigma_{\mathrm{cut}}}} \sum_{j=1}^{N_{\mathrm{sites}}^{\mathrm{CN}}} \times \delta(|\boldsymbol{R}_i - \boldsymbol{r}_j^{\mathrm{CN}}| - r) h(\sigma_i, \sigma_{\mathrm{cut}}) \quad (3.1)$$

where $N_{\mathrm{voids}}^{\sigma_{\mathrm{cut}}}$ is the total number of voids identified in the system above a certain cutoff radius, σ_{cut}, $N_{\mathrm{sites}}^{\mathrm{CN}}$ is the number of cation sites of a specific coordination number (CN) and $\boldsymbol{R}^i$ and $\boldsymbol{r}^j$ are their respective positions. In order to understand the relationship between the five-coordinate sites and the larger voids (which define the cavities in the low density structures) we choose to 'colour' only the voids above a certain size (σ_{cut}) by setting $h(\sigma_i, \sigma_{\mathrm{cut}}) = 1$ if $\sigma_i > \sigma_{\mathrm{cut}}$ and zero otherwise. Fig. 4 shows $g_{\mathrm{cV}}(r, \sigma_{\mathrm{cut}})$ calculated for no cutoff and for cutoffs of 7.5 and 10 a_0 respectively. The latter corresponds only to the large cavities from Fig. 1 whilst the former includes a significant number of smaller holes. For no cutoff the four- and five-coordinate sites show a similar relationship to the voids, as we would expect. At the smaller cutoff the four-coordinate function is a near step function indicating no spatial preference of these sites with respect to voids above 7.5 a_0. However, the low 'intensity' of the distribution function at low separations (corresponding to the edges of the hole) for the five-coordinate sites indicate that they prefer to stay away from these holes. This behaviour is more distinct at the higher cutoff when even the four-coordinate sites start to show a slight preference for being away from the void edges.

Fig. 5 shows a molecular graphics snapshot of the SiO_2 simulation cell at 1.6 g cm^{-3}. A large cavity is clearly visible

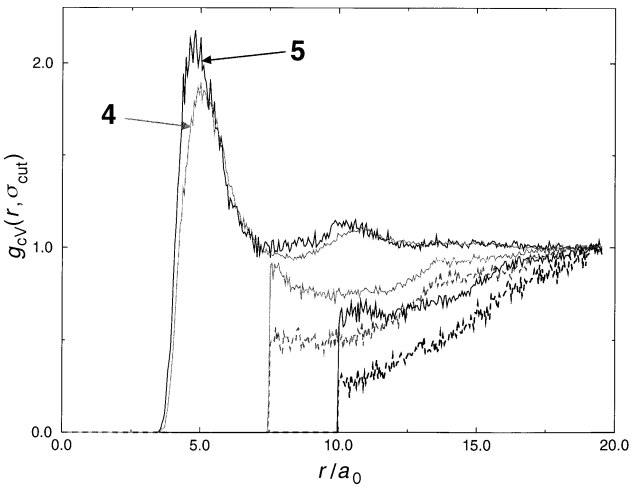

Fig. 4 Void–cation radial distribution functions for voids coloured according to a specific size range (σ_{cut}) with cations coloured according to coordination number. Key: solid black line (labelled 5), five-coordinate cation (labelled 5), $5 + \sigma_{\mathrm{cut}} = 0$; light solid line (labelled 4), $4 + \sigma_{\mathrm{cut}} = 0$; light solid line, $4 + \sigma_{\mathrm{cut}} = 7.5\ a_0$, light dashed line, $5 + \sigma_{\mathrm{cut}} = 7.5\ a_0$; black solid line, $4 + \sigma_{\mathrm{cut}} = 10\ a_0$; black dashed line, $5 + \sigma_{\mathrm{cut}} = 10\ a_0$.

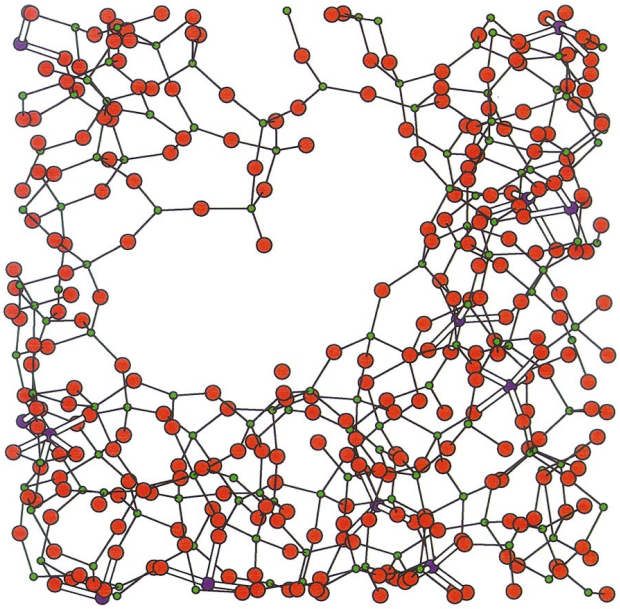

Fig. 5 Molecular graphics 'snapshot' of the SiO_2 model at 1.6 g cm^{-3}. Key: large red circles, O^{2-}; blue, five-coordinate Si^{4+}; green, all other Si^{4+}. A large cavity is clearly seen with the five-coordinate sites highlighted to show how they 'avoid' the cavity.

in the cell. The five-coordinate sites have been highlighted showing how they avoid the void edges. As a result of this analysis we can postulate that the diffusivity in the low density silicas arises largely from motion in the bulk-like regions. The five coordinate sites tend to stay away from the edges of the large holes instead preferring to move in the bulk 'channels'. Smaller additional simulations at even lower densities show that the ion diffusivity falls at these reduced densities as the width of these channels contracts. Previous studies[22] have shown that the fractal nature of these systems persists to much lower densities than those considered here (<0.1 g cm^{-3}) without the formation of droplets expected for more Lennard-Jonesian systems. The precise nature of (and possible changes in) the diffusivity mechanism and the relationship to the increase in the internal surface area (reduced dimensionality) is a matter of ongoing study.

4 Total and partial edge-sharing networks

Both $BeCl_2$ and $ZnCl_2$ may be thought of as formed from linked MX_4 tetrahedra but with resulting structures quite different from that of silica. The structure of $BeCl_2$ is based almost totally on edge-sharing tetrahedra in both the crystal and liquid states[3] which, in this stoichiometry, lead to long chains of such linked tetrahedra terminated by three-coordinate Be^{2+} 'end groups'. As a result each chain is charge neutral. In this ('polymeric') structure the IRO arises from inter-chain correlations (and so is, once again, predominantly reflected in the cation–cation correlations).[3]

$ZnCl_2$ can be considered as structurally intermediate between the two extremes of pure edge- and pure corner-sharing tetrahedra. The Zn—Cl—Zn bridging bond angles are in between those of SiO_2 and $BeCl_2$ [$\theta(ZnCl_2)$ *ca.* 110° compared with *ca.* 150° for SiO_2 and *ca.* 80° for $BeCl_2$] with a structure comprising of a mixture of (dominating) corner and edge-sharing tetrahedra. As mentioned in the Introduction the 'transition' from the pure corner-sharing network observed for SiO_2 and the pure edge-sharing in $BeCl_2$ *via* the intermediate $ZnCl_2$ can be understood in terms of anion polarization effects. Both $ZnCl_2$ and $BeCl_2$ are studied as liquids at ambient pressure.

4.1 Real space void distributions

Fig. 6 shows the circumsphere radius distribution for $ZnCl_2$ studied using a RIM and PIM (see ref. 4) and $BeCl_2$ studied using a PIM only. The $ZnCl_2$ RIM distribution is very similar to the ambient pressure distributions observed for SiO_2 in the previous section. The PIM distribution has a similar shape to that of the RIM but is significantly broader (FWHM of *ca.* 1.39 a_0 compared with *ca.* 1.09 a_0) reflecting the greater range of void sizes and suggesting a reduced uniformity of the cation subdensity. The circumsphere radius distribution for $BeCl_2$ is significantly broader than either the RIM or PIM $ZnCl_2$ curves with a FWHM of *ca.* 2.50 a_0 which indicates an even less isometric structure than in the $ZnCl_2$ PIM.

The broader distribution for $BeCl_2$ reflects the inherent chain structure. The chains are individually charge neutral and so the inter-chain interactions are dominated by the short-range (overlap) and attractive dispersive interactions. As a result the system structure can be thought of in terms of 'strong' bonds, which hold the individual (one-dimensional) chains together, and the 'weak' bonds which act between these chains. The chain–chain spatial correlations are much broader than in the more rigid $ZnCl_2$, and it is this which leads directly to the significantly broader void size distribution.

Fig. 7 shows the radial distribution function, g_{VV} corresponding to the pairwise spatial distribution between the circumspheres for $ZnCl_2$ and $BeCl_2$ respectively.

$$4\pi r^2 g_{VV}(r) = \frac{V}{N_{voids}^{\sigma_{cut}}} \sum_{i=2}^{N_{voids}^{\sigma_{cut}}} \sum_{j=1}^{j=i-1} \times \delta(|\boldsymbol{R}_i - \boldsymbol{R}_j| - r) h(\sigma_i, \sigma_{cut}) h(\sigma_j, \sigma_{cut}) \quad (4.1)$$

$$\times \delta(|\boldsymbol{R}_i - \boldsymbol{R}_j| - r) h(\sigma_i, \sigma_{cut}) h(\sigma_j, \sigma_{cut}) \quad (4.1)$$

The functions increase in intensity as $r \to 0$ (unlike atomic pair distribution functions) reflecting the fact that many circumspheres may occupy a 'single' void. Again, extra information is extracted by considering the spatial correlations between circumspheres above a certain cutoff size, σ_{cut}. As this cutoff radius is increased the $ZnCl_2$ PIM distribution function peak shifts to longer range and becomes much sharper. In contrast the $BeCl_2$ distributions are less featured.

The increased sharpness of the $ZnCl_2$ pair distribution function with increasing cutoff indicates that the larger voids are spatially ordered so as not to interpenetrate. The peak positions themselves occur at intermediate (>5 Å) length scales of the distribution of ionic positions.[4,23] The $BeCl_2$ radial distribution functions show a very low intensity peak at longer range. More significantly, however, these functions decay from

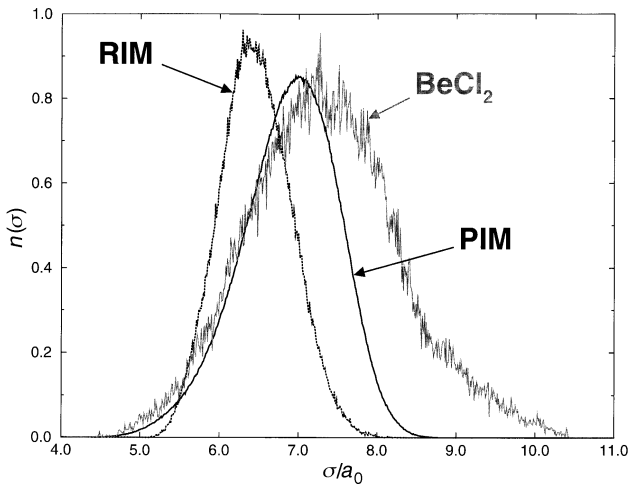

Fig. 6 Circumsphere radii distributions for $ZnCl_2$ (dark lines labelled RIM and PIM) and $BeCl_2$ (PIM only), light line

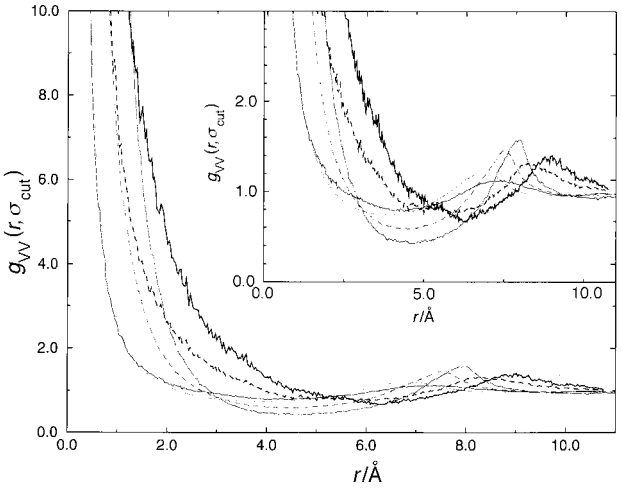

Fig. 7 Void–void pair distribution functions, $g_{VV}(r)$, for $ZnCl_2$ and $BeCl_2$ over a range of void sizes, σ_{cut}. Key: $ZnCl_2$; light solid line, $\sigma_{cut} = 0$; light dashed line, $\sigma_{cut} = 0$; light dashed line, $\sigma_{cut} = 7.0\ a_0$; thick light line, $\sigma_{cut} = 7.5\ a_0$. $BeCl_2$; black solid line, $\sigma_{cut} = 0$; dark dashed line, $\sigma_{cut} = 7.5\ a_0$; thick dark line, $\sigma_{cut} = 8.0\ a_0$. The inset shows an enlarged region of the main plot.

$R = 0$ much more slowly than those for $ZnCl_2$, indicating that large voids may be found relatively freely around each other with less structure than for the $ZnCl_2$ case.

We again consider the pair relationship between specifically coordinated cations and voids, coloured according to radius [eqn. (3.1)]. The three- and four-coordinate Be^{2+} ion (the 'end-groups' and main chain units respectively) distributions show no significant differences regardless of the circumsphere size. This shows that the void structure is effectively averaged out by the relatively free motion of the cation chains with respect to each other. If, for example, the chains were to be moving around in a highly correlated fashion then one might see a correlation between the larger voids and the three-coordinate endgroups reflecting the larger holes in the system at the chain ends.

Whilst Fig. 7 indicates a clear difference between the two systems, it does not tell us the nature of any ordering in the $BeCl_2$ case. Fig. 8(*a*) and (*b*) show snapshots of the $ZnCl_2$ and $BeCl_2$ PIM void centres joined if less than 4 a_0 apart. The $ZnCl_2$ distribution shows significant clustering as indicated by the ordered radial distribution function. The $BeCl_2$ system, on the other hand, displays more long 'strand-like' structures formed from voids linked together. The distribution of separations in these strings leads to the relatively unstructured radial distribution function, with the strings themselves indicative of the chain structure of the ions themselves.

4.2 Reciprocal space void distributions and the signature of IRO in $ZnCl_2$, $BeCl_2$ and SiO_2

The interplay between the ion structure, as governed by the ion positions, and the void structure, can also be studied in reciprocal space. In a simple (one component) atomic liquid the nearest-neighbour (short-range) length scale, l, is related simply to the position of the principal peak position in the static structure factor, $k_{PP} \approx 2\pi/l$. Geometrical (packing) requirements dictate that this length also controls the real space structure at longer range so that there are no reciprocal space features at lower k than k_{PP}. In the (binary) systems of interest here, the basic structural units can be considered to be the cation-centred polyhedra (analogous to the atoms of the one-component system) and we therefore consider the cation–cation partial structure factors to see how these units are organized through space. Unlike the one-component system, the nearest-neighbour cation–cation separation, l_{++}, does not necessarily control the arrangement of the tetrahedra at longer range, a second (intermediate-ranged) length scale may

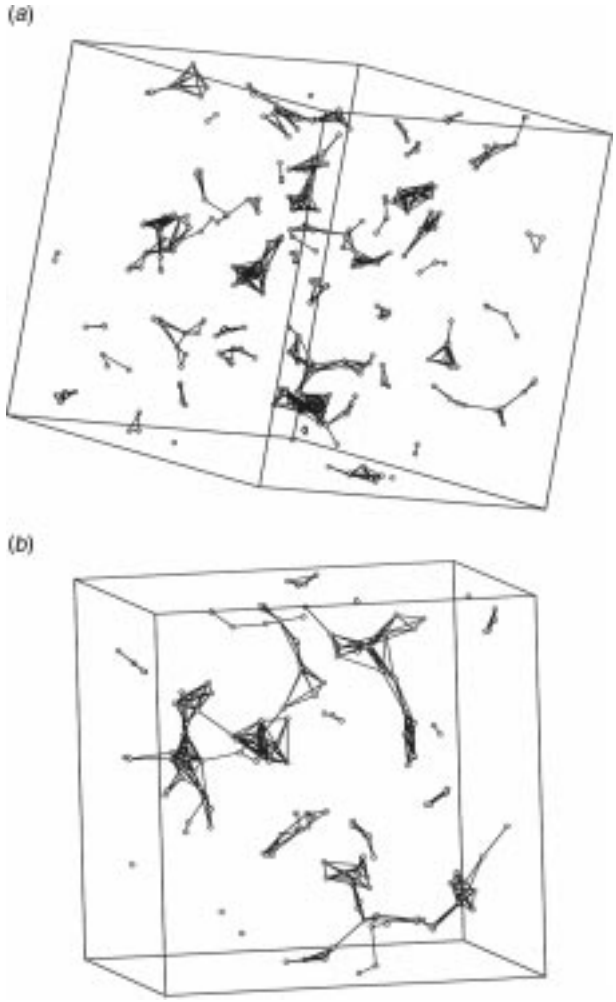

Fig. 8 Molecular graphics 'snapshots' of the void centre positions for (*a*) $ZnCl_2$ and (*b*) $BeCl_2$. The voids for circumsphere radii $>8\ a_0$ are shown and are connected if $<4\ a_0$ apart.

arise from the polyhedral connectivity. This then may be associated with a reciprocal space feature (the first sharp diffraction peak, or FSDP) at lower k than the principal peak, for which (in our terminology) k_{PP} is *ca.* $2\pi/l_{++}$.

This situation is illustrated by the upper panel of Fig. 9, which shows that the cation–cation structure factors for $ZnCl_2$ from the RIM and PIM simulations (at the same density) exhibit considerable differences as a consequence of the polarization effects on the polyhedral (tetrahedra) connectivity. Also indicated in the figure (by arrows) are the positions of the first two peaks in structure factors calculated from simply the first peaks of the radial distribution functions of the fluids, *i.e.* information on the nearest-neighbour separation l_{ZnZn} is included, but not on longer length scales. To do this we simply transform a $g(r)$ constructed from the cation–cation radial distribution function for r up to the point at which it equals unity on the high r side of the first peak and which is then set to one for all r values greater than this value. In the RIM, the arrows correspond well with the positions of the first two peaks in the calculated structure factor, indicating that the nearest neighbour separation controls the structure on all length scales and implying a simplicity in the network connections. When polarization effects are introduced, the principal peak in the RIM is split into two peaks. The new principal peak ($k_{PP} \approx 2\pi/l_{Zn-Zn}$ for the PIM) has moved to a larger k than in the RIM, a direct result of the closer approach (reduction in l_{Zn-Zn}) of pairs of Zn^{2+} ions brought about by the bending of the bond between adjacent tetrahedra.[1] At smaller k a new peak (the FSDP) has appeared at $k_{FSDP} \approx 1$ $Å^{-1}$.

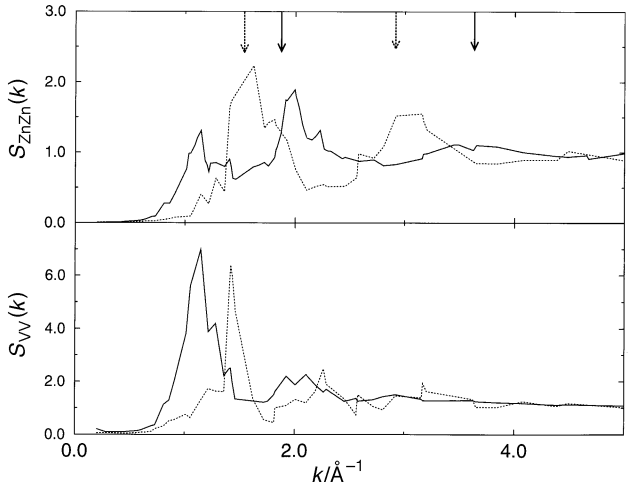

Fig. 9 Void–void structure factors (bottom) for $ZnCl_2$ RIM (dotted line) and $ZnCl_2$ PIM (solid line) compared with the cation–cation functions (top). The arrows indicate the positions of the first two peaks in the structure factor derived from the main peak in g_{ZnZn} as explained in the text.

To understand the significance of the new length scale ($2\pi/k_{FSDP}$), which is not readily identified in the real space distribution function,[24] it is of interest to see if such low k features may be associated with the void structure. To this end we can define a static structure factor as if the void centres were radiation-scattering particles

$$S_{VV}(k) = \frac{1}{N_V}\left\langle \sum_{i,j=1}^{N_V} \exp(i\boldsymbol{k}\boldsymbol{R}^{ij}) \right\rangle \qquad (4.2)$$

S_{VV} for $ZnCl_2$ in the RIM and the PIM is shown in the lower panel to Fig. 9. S_{VV}^{PIM} shows two main peaks located in the same places as those in S_{ZnZn}^{PIM} (at k_{FSDP} and k_{PP}) with that at the FSDP by far the most intense, indicating that the new length scale seen in the FSDP of the cation–cation structure factor is that which dominates the ordering of the voids. Such a picture is very much in the spirit of the glass models proposed by Elliott and co-workers.[25] The first feature in S_{VV}^{RIM}, on the other hand, appears close to the principal peak observed in S_{ZnZn}^{RIM}, showing that there is no new length scale associated with the voids in this case, the positions of voids and cations arises simply from coulomb-driven stacking of the tetrahedra.

Fig. 10 shows S_{BeBe} (upper panel) and S_{VV} for the $BeCl_2$ PIM simulation. S_{BeBe} shows a structure like that in $ZnCl_2$ with a principal peak corresponding to nearest-neighbour

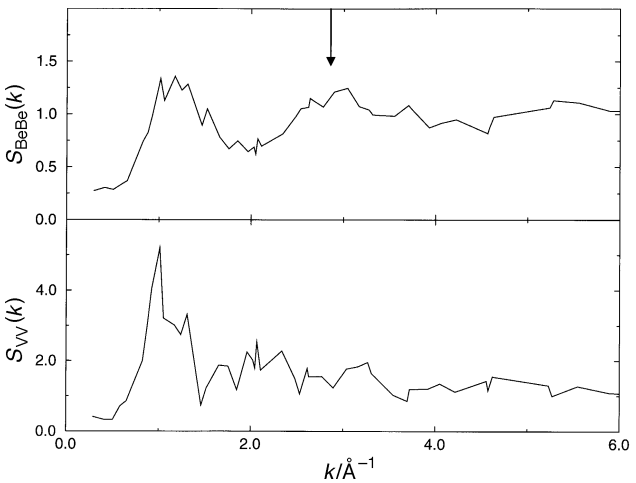

Fig. 10 Void–void structure factors (bottom) for $BeCl_2$ compared with the cation–cation functions (top). The arrow indicates the position of the first peak in the structure factor derived from the main peak in g_{BeBe}.

cation–cation interactions (again indicated by an arrow in the figure at *ca.* $2\pi/l_{Be-Be}$), and a FSDP corresponding to longer range correlations. Following the above discussion of the real space structure, we would regard l_{Be-Be} as an intra-chain separation and the FSDP to arise from interchain correlations. It is of interest to see how this different real-space arrangement is reflected in the relationship of the void and cation structure factors. Although the first peak in S_{VV} (again at $k \approx k_{FSDP}$ for S_{BeBe}) is like that in $ZnCl_2$ in terms of its intensity and position, unlike $ZnCl_2$ there is no peak in S_{VV} at the principal peak position of S_{BeBe}. The peak in S_{VV} at k_{FSDP} in $BeCl_2$ arises through the spatial correlations between voids existing between chains of cations and therefore in the same position as the inter-chain Be—Be correlations. There is no analogue in the void–void distribution of the local structure responsible for l_{Be-Be}; this arises from the separation of neighbouring tetrahedra along the 'polymer' chains, these chains do not contain any cation voids.

Fig. 11 compares the void structure factors defined above with the cation–cation function at densities of 5.2 g cm^{-3} [(Fig. 11(a)] and 2.2 g cm^{-3} [(Fig. 11(b)] for SiO_2. At the higher density, we recall that the local structural motif is octahedral and that the behaviour of the simulated fluid is like that of a simple 'fragile' melt, dominated by the coulombic (and not polarization) interactions. In this case, the position of the first peak in S_{VV} corresponds to that of the principal peak in S_{SiSi} (the position of the peak arising from the first neighbour peak in $g_{SiSi}(r)$ is again indicated by an arrow). This is analogous to the situation seen in $ZnCl_2$ in the RIM, where there is only one length scale set by the nearest-neighbour

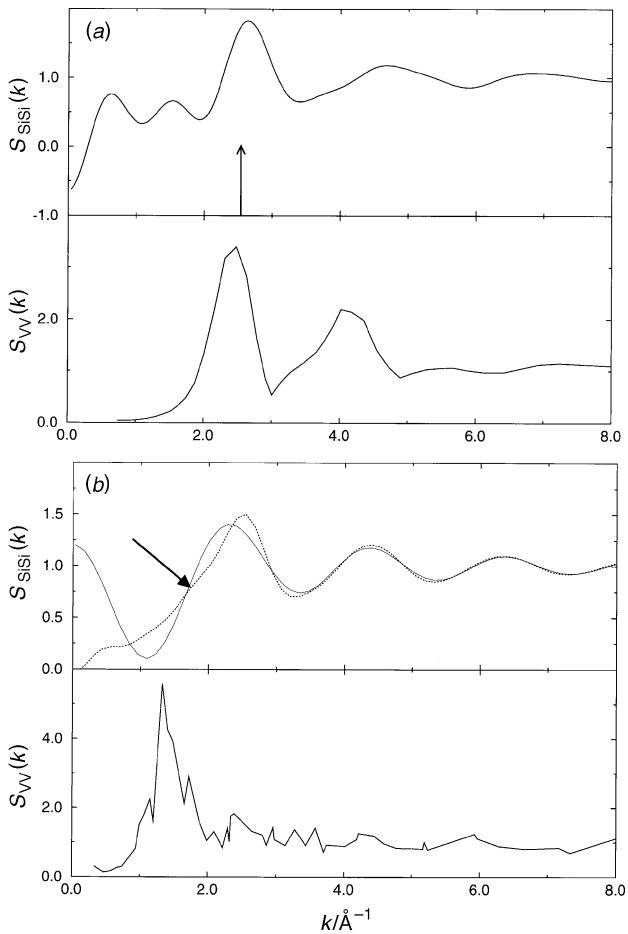

Fig. 11 Void–void structure factors (bottom), $S_{VV}(k)$, for SiO_2 at (*a*) 5.2 g cm^{-3} and (*b*) 2.2 g cm^{-3} compared with the cation–cation functions (top). The arrow in (*a*) highlights the shoulder (see text) whilst the solid line in (*b*) is the structure factor derived from the transformation of the first peak in g_{SiSi} only.

separation of the polyhedral units. At the normal liquid density (2.2 g cm^{-3}), where local tetrahedral order dominates, some new features emerge, not encountered in the previous examples. Unlike $ZnCl_2$, we do not see a sharp distinction between an FSDP and a principal peak (identified as occurring at *ca.* $2\pi/l_{Si-Si}$). In S_{SiSi} the position of the main peak no longer coincides with that derived from the nearest-neighbour peak in g_{SiSi}; in this case we show the whole of the transform of the first peak of g_{SiSi} as the solid line in the figure. This transform has a peak position significantly lower than that of the main peak in S_{SiSi} and appears to be responsible for the 'prepeak' which appears only as a shoulder (indicated by the arrow) on the leading edge of the main peak at these elevated temperatures (this feature becomes more pronounced at lower temperatures[26]). Hence, in this case, it appears to be the nearest-neighbour separation which is reflected in the position of the lowest k feature, and the dominant feature of the structure factor at somewhat higher k is indicative of a more complex spatial arrangement of cations. In considering the relationship to the void structure, we see a strong first peak in S_{VV} which, unlike the $BeCl_2$ and $ZnCl_2$ cases, is not associated with a distinctive and well resolved feature in S_{SiSi}. The position of the peak in S_{VV} seems to be associated with the shoulder in S_{SiSi} and not the main peak.

It seems clear from this consideration of the void structure factors and the relationship of the positions of peaks in the cation structure factors to the real-space distance of closest approach that the low k features in the structure factor of SiO_2 at normal liquid density have a different origin to the $ZnCl_2$, $BeCl_2$ and dense SiO_2 cases considered above. In these latter cases, the void structure factor is a useful adjunct to the interpretation of the observable cation–cation structure factor. In normal SiO_2 it merely indicates an additional degree of complexity in the tetrahedral correlations at intermediate range. Further work is in progress to clarify the origin of these differences.

Conclusions

We have shown how an analysis of the voids in the tetrahedrally based liquids SiO_2, $ZnCl_2$ and $BeCl_2$ acts as a useful adjunct to the more normally discussed structural properties of liquids in interpreting the origin of unusual properties of these liquids associated with their network-forming character. The Voronoi–Delauney analysis of the voids is readily applied to the atomic positions obtained in the course of a computer simulation and is particularly useful for liquids of this type because it gives a readily visualized measure related to the intermediate range order (IRO) in these systems. The IRO is itself strongly affected by the elementary polarization interactions and is therefore influenced by the relative size of the cation and anion and by the polarizability of the anion. Simultaneous examination of changes in void properties and coordination numbers of SiO_2 under extreme pressure and tension gives a vivid picture of the collapse and rupture of the network and allows an interpretation of the anomalous behaviour of the ion diffusivity. In $ZnCl_2$ and $BeCl_2$ the structure factor calculated for the voids shows a principal peak in common with the first sharp diffraction peak (FSDP) of the cation–cation structure factor, and thereby provides a ready interpretation of this experimentally observable consequence of the IRO. In SiO_2 the relationship of the void and ionic structure factors is less direct and suggests a different origin for the FSDP in this case.

References

1 P. A. Madden and M. Wilson, *Chem. Soc. Rev.*, 1996, **25**, 339.
2 M. Hemmatti and C. A. Angell, *J. Non-Cryst. Solids*, 1997, **217**, 236.
3 M. Wilson and P. A. Madden, *Mol. Phys.*, 1997, **92**, 197.
4 M. Wilson and P. A. Madden, *Phys. Rev. Lett.*, 1998, **80**, 532.
5 F. Sciortino, A. Geiger and H. E. Stanley, *J. Chem. Phys.*, 1992, **96**, 3857.
6 P. H. Poole, M. Hemmati and C. A. Angell, *Phys. Rev. Lett.*, 1997, **79**, 2281.
7 M. Wilson, M. C. C. Ribeiro and P. A. Madden, to be published.
8 L. V. Woodcock, C. A. Angell and P. Cheeseman, *J. Chem. Phys.*, 1976, **65**, 1565.
9 M. Wilson, P. A. Madden, M. Hemmati and C. A. Angell, *Phys. Rev. Lett.*, 1996, **77**, 4023.
10 M. Wilson, P. A. Madden, N. C. Pyper and J. H. Harding, *J. Chem. Phys.*, 1996, **104**, 8068.
11 M. Wilson and P. A. Madden, *Faraday Discuss.*, 1997, **106**, 339.
12 A. J. Rowley, P. J. Jemmer, M. Wilson and P. A. Madden, *J. Chem. Phys.*, in press.
13 G. H. Wolf, S. Wang, C. A. Herbst, D. J. Durben, W. F. Oliver, Z. C. Kang and K. Halvorson, *High Pressure Res.*, 1992, 503.
14 D. L. Lacks and R. G. Gordon, *Phys. Rev. B.*, 1993, **48**, 2889; *J. Geophys. Res. B*, 1993, **98**, 22 147.
15 Y. I. Naberukhin, V. P. Voloshin and N. N. Medvedev, *Mol. Phys.*, 1991, **73**, 917.
16 D. S. Corti, P. G. Debenedetti, S. Sastry and F. H. Stillinger, *Phys. Rev. E*, 1997, **55**, 5522.
17 J. D. Bernal, *Proc. R. Soc. London, Ser. A*, 1964, **280**, 299; J. L. Finney, *ibid*, 1970, **319**, 495.
18 A. Navrotsky, *MRS Bull.*, 1997, **22**, 35.
19 J. P. Itie, A. Polian, G. Calas, J. Petiau, A. Fontaine and H. Tolentino, *Phys. Rev. Lett.*, 1989, **63**, 398.
20 C. A. Angell, *J. Phys. Chem. Solids*, 1988, **49**, 863.
21 J-L. Barrat, J. Badro and P. Gillet, *Mol. Sim.*, 1997, **20**, 17.
22 J. Kieffer and C. A. Angell, *J. Non-Cryst. Solids*, 1988, **106**, 336.
23 M. Wilson and P. A. Madden, *Phys. Rev. Lett.*, 1994, **72**, 3033.
24 P. S. Salmon, *Proc. R. Soc. London, Ser. A.*, 1992, **437**, 591; *ibid.*, 1994, **445**, 351.
25 S. N. Taraskin, S. R. Elliott and M. Klinger, *J. Non-Cryst. Solids*, 1995, **193**, 263; J. H. Lee and S. R. Elliott, *ibid*, 1995, **193**, 133; A. Ulherr and S. R. Elliott, *ibid.*, 1995, **193**, 98.
26 P. Vashishta, R. K. Kalia, J. P. Rino and I. Ebbsjö, *Phys. Rev. B*, 1990, **41**, 12 197.

Paper 8/00365C; *Received* 13*th January*, 1998